Effective interaction for $^{16}O(p,p')$ at $E_p = 318$ MeV

J. J. Kelly, A. E. Feldman, B. S. Flanders,[a] and H. Seifert
Department of Physics and Astronomy, University of Maryland, College Park, Maryland 20742

D. Lopiano,[b] B. Aas,[c] A. Azizi,[d] G. Igo, G. Weston,[e] C. Whitten, and A. Wong[f]
Department of Physics, University of California at Los Angeles, Los Angeles, California 90024

M. V. Hynes and J. McClelland
Los Alamos National Laboratory, Los Alamos, New Mexico 87545

W. Bertozzi, J. M. Finn,[g] C. E. Hyde-Wright,[h] R. W. Lourie,[i] and P. E. Ulmer[j]
Department of Physics and Laboratory for Nuclear Science, Massachusetts Institute of Technology, Cambridge, Massachusetts 02139

B. E. Norum
Department of Physics, University of Virginia, Charlottesville, Virginia 22901

B. L. Berman
Department of Physics, George Washington University, Washington, D.C. 20052
(Received 8 November 1990)

We report new cross-section and analyzing power data for the excitation by 318 MeV protons of 20 states of ^{16}O below 14 MeV. The data for normal-parity isoscalar excitations are compared with calculations based upon the nonrelativistic impulse approximation using both density-independent and density-dependent interactions in the local-density approximation. These comparisons clearly indicate that density-dependent modifications of the effective interaction are required. Although the Paris-Hamburg, Nakayama-Love, and Ray interactions all predict significant medium modifications, none describes the data particularly well. Therefore, we fitted an empirical effective interaction to the data for five inelastic transitions simultaneously using a self-consistency cycle that maintains consistency between transition potentials and microscopic distorting potentials. This interaction describes the inelastic data as well as elastic data and data for ^{40}Ca which were not included in the fitting procedure. Therefore, the local-density approximation is supported by the phenomenology. However, medium modifications of the effective interaction are substantially stronger than predicted and persist to low density. The optical potentials are similar to the Schrödinger-equivalent potentials from the relativistic IA2 model, showing that the equivalent density dependence due to virtual $N\bar{N}$ pairs is comparable to the short-range repulsion fitted to inelastic-scattering data.

I. INTRODUCTION

For energies below about 200 MeV, the nonrelativistic impulse approximation (NRIA) requires strong medium modifications of the two-nucleon effective interaction to describe elastic scattering and inelastic scattering to normal-parity states of the target nucleus.[1-4] The density dependence of the effective interaction results primarily from Pauli blocking and self-energy corrections and is described qualitatively by nuclear matter calculations and the local-density approximation (LDA).[5-8] However, the detailed predictions of these models vary considerably with the approximation scheme, and a sound theoretical method for evaluating these effects has not yet been established. Therefore, it has been necessary to develop an empirical effective interaction, motivated by the nuclear matter theory, whose parameters can be fitted to a large body of inelastic-scattering data. Empirical effective interactions have been fitted for several energies below 200 MeV and have been shown to provide an excellent description of the data.[3,4]

The strongest density dependence is exhibited by the central spin-independent isoscalar component of the effective interaction. The effect of Pauli blocking is represented by a damping factor applied to the imaginary central interaction. The effect of short-range correlations upon the real central interaction can be represented by a short-range repulsive interaction proportional to density.

As the energy increases, the effect of Pauli blocking upon the absorption cross section is expected to decrease with energy as E^{-1} in accordance with the phase-space model of Clementel and Villi.[9] More detailed nuclear matter calculations tend to confirm that the density dependence of the imaginary central component of the

effective interaction decreases rapidly with energy. On the other hand, the density dependence of the real central interaction is expected to vary more slowly with energy. Hence, we might expect that, by 300 MeV, the imaginary interaction will become similar to the free interaction whereas the real interaction may retain significant density dependence. However, the three nuclear matter calculations presently available for the 300-MeV regime differ considerably in their predictions for the real central interaction.[6–8] Therefore, a phenomenological analysis is still necessary.

At 500 MeV and above, the relativistic impulse approximation (RIA) has been shown to give a description of elastic scattering, especially spin observables, that is superior to the NRIA based upon the free interaction.[10–13] Alternatively, we have shown that the empirical interaction fitted to inelastic-scattering data also gives an excellent description of elastic scattering that is at least as accurate as the RIA for spin observables.[14] However, the density dependence of the empirical effective interaction is surprisingly strong. Therefore, it is of interest to compare these approaches for an intermediate energy such as 318 MeV.

In this paper we report new data for elastic and inelastic scattering of 318-MeV protons by ^{16}O. These data will be compared with NRIA calculations based upon the Franey-Love t matrix[15] and with LDA calculations based upon several density-dependent effective interactions.[6–8] An empirical effective interaction is also fitted to the data and compared with the IA2 model.[12]

The experiment is described in Sec. II. The various models of the effective interaction are compared in Sec. III. Calculations based upon these models are compared with the data in Sec. IV and our conclusions are summarized in Sec. V.

II. EXPERIMENT

The experiment was performed using 318-MeV polarized protons provided by the Los Alamos Meson Physics Facility (LAMPF). The beam current was monitored by a pair of ionization chambers following the target within the scattering chamber. These monitors were normalized by comparing elastic pp measurements made with a thin CH_2 target with calculations based upon Arndt phase shifts.[16] The polarization was monitored by a continuous in-line polarimeter described in Ref. 17 and was typically in the range 0.75–0.86. Several beryllium oxide (BeO) foils with thicknesses between 23.7 and 101.7 mg/cm^2 were used as targets. The various targets gave cross sections which agreed within the estimated ±5% normalization uncertainty. In addition, two Be foils (26.8 and 47.3 mg/cm^2) were used to collect data upon the beryllium continuum below the oxygen states of interest.

Scattered protons were analyzed using the high-resolution spectrometer (HRS) and detected by the standard focal-plane array described in Ref. 18. From known spectrometer constants, the beam energy was found to be in the range 317.4±0.4 MeV. For each spectrometer setting, the events were sorted into three equally spaced bins of laboratory scattering angle that were ±0.3° wide and covered the useful acceptance. The spectra were analyzed with the ALLFIT program and methods described in Refs. 2, 4, and 19. A typical fitted spectrum is shown in Fig. 1, which illustrates the states analyzed herein. The ^9Be continuum was described using the positions and widths deduced by Dixit *et al.*[20] Narrow peaks of ^{16}O were described by the standard hyper-Gaussian line shape. Peaks with intrinsic widths larger than 20 keV were described as Lorentzian shapes convoluted with a resolution function based upon the narrow peaks. The positions and widths compiled in Ref. 21 were used. The positions of closely spaced peaks were constrained to tabulated values. Further details may be found in Ref. 22.

Data for 20 states below 14 MeV were collected for laboratory angles between 5° and 47° in steps of 2°–3°, spanning the momentum transfer range $0.32 \le q \le 3.18$ fm^{-1}. In this paper we focus upon the normal-parity isoscalar states 0_1^+ (0.0 MeV), 0_2^+ (6.049 MeV), 0_3^+ (12.053 MeV), 1_1^- (7.117 MeV), 2_1^+ (6.917 MeV), 2_2^+ (9.847 MeV), 2_3^+ (11.521 MeV), 3_1^- (6.130 MeV), and 4_1^+ (10.353 MeV). Data were also collected for the 2_1^- state at 8.872 MeV, the 0_1^- state at 10.952 MeV, a $(3_1^+ 4_2^+)$ doublet at 11.09 MeV, and seven additional states between 12.4 and 13.9 MeV. Complete data tables are on deposit with the Physics Auxiliary Publication Service (PAPS).[23]

III. MODELS OF THE EFFECTIVE INTERACTION

A. Local-density approximation

The approximation scheme we employ to evaluate the folding model of nucleon-nucleus scattering has been

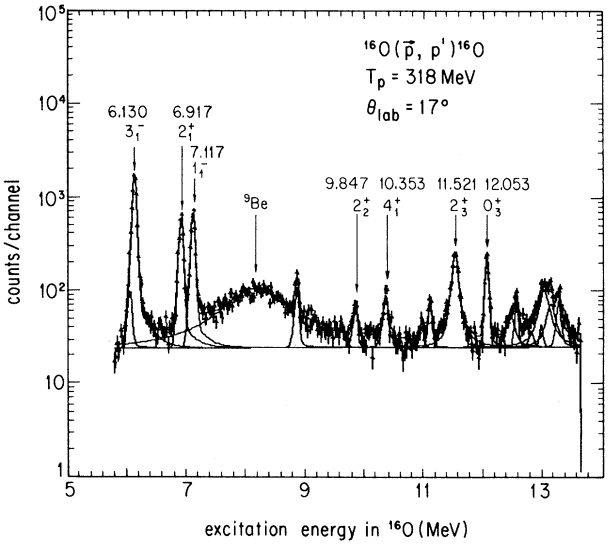

FIG. 1. Typical fitted spectrum for $^{16}O(\vec{p},p')$ at $T_p=318$ MeV obtained with a BeO target at a laboratory scattering angle of 17°. The ^{16}O states considered in this paper are labeled with multipolarity and excitation energy in units of MeV. Note that the 0_3^+ and 1_1^- states, which have strong interior transition densities, are quite prominent. A broad bump corresponding to two states in ^9Be is also indicated.

presented in considerable detail in Refs. 2 and 3. In this section it is sufficient to outline those aspects of the model that are relevant to subsequent discussions.

In this paper we focus upon normal-parity isoscalar transitions for which electroexcitation measurements determine the longitudinal form factor for $q \leq 2.7$ fm^{-1} with good accuracy.[24] Furthermore, the transverse form factors for these states are all very small. Hence, we assume that all spin and current densities, including those not sampled by electron scattering, are negligible. This assumption is justified by the fact that spin and current densities are systematically suppressed for collective excitations and by the fact that the interaction that couples to the matter density is much stronger than the interactions that probe these spin and current densities. Similarly, the matter interaction is much stronger than the isovector interaction and charge symmetry ensures that the proton and neutron transition densities for isoscalar excitations of self-conjugate targets are very nearly equal. Therefore, the proton transition densities obtained by unfolding the nucleon finite size from the transition charge densities measured with electron scattering suffice to determine all nuclear structure quantities required to analyze the transitions of interest in terms of the effective interaction.

The effective interaction for normal-parity isoscalar transitions with negligible spin and current contributions reduces to

$$t(q)=t^{C}(q)+it^{LS}(q)\boldsymbol{\sigma}\cdot\mathbf{n} , \tag{1}$$

where $\boldsymbol{\sigma}$ describes the projectile spin and $\mathbf{n}$ is the unit vector normal to the scattering plane. The t matrix in the nucleon-nucleus (NA) frame is related to that in the nucleon-nucleon (NN) frame by a Jacobian denoted η. Following the notation of Ref. 2, it is convenient to introduce the auxiliary quantity τ^{LS} via

$$t^{LS}=\frac{-qQ\tau^{LS}}{2}=-(k^2\sin\theta)\tau^{LS} , \tag{2}$$

where $\mathbf{q}=\mathbf{k}_i-\mathbf{k}_f$ is the direct and $\mathbf{Q}=\mathbf{k}_i+\mathbf{k}_f$ is the exchange momentum transfer. We evaluate exchange contributions using a local approximation.

Normal-parity isoscalar transitions are excited by scattering potentials of the form

$$U(\mathbf{r})=U^{Z}(\mathbf{r})+U^{C}(\mathbf{r})+\boldsymbol{\nabla}F^{LS}(\mathbf{r})\otimes\frac{1}{i}\boldsymbol{\nabla}\cdot\boldsymbol{\sigma} , \tag{3}$$

where U^Z is the potential obtained by folding the Coulomb interaction with either the ground-state or transition charge density. The central and spin-orbit potentials U^C and F^{LS} are obtained by folding the matter transition density ρ_J with central and spin-orbit components of the effective interaction t^C and τ^{LS} according to

$$U_J^C(r)=\frac{2}{\pi}\int dq\, q^2 j_J(qr)\eta t^C(q,\rho_G(r))\rho_J(q) , \tag{4a}$$

$$F_J^{LS}(r)=\frac{2}{\pi}\int dq\, q^2 j_J(qr)\eta \tau^{LS}(q,\rho_G(r))\rho_J(q) , \tag{4b}$$

where ρ_G is the local ground-state matter density. For simplicity, the effective interaction is evaluated for the local density at the site of the projectile; the differences obtained for alternative choices of local density, such as the position of the struck nucleon or the two-body center of mass, are much smaller than the ambiguities due to the choice of interaction.[2]

Similarly, the elastic optical potential has the form

$$U(r)=U^{Z}(r)+U^{C}(r)+U^{LS}(r)\mathbf{L}\cdot\boldsymbol{\sigma} , \tag{5}$$

where

$$U^{LS}(r)=\frac{1}{r}\frac{\partial F^{LS}}{\partial r} . \tag{6}$$

For consistency with previous analyses, the ground-state density tabulated in Ref. 25 is used. However, an earlier density due to Miska *et al.*[26] produces a stronger maximum in the form factor near 3 fm^{-1} and gives somewhat better agreement with the large-angle elastic-scattering data at this and lower energies. Fortunately, this minor ambiguity does not affect the inelastic-scattering calculations and thus will not affect any of our conclusions.

According to Cheon *et al.*,[27] the density dependence of the effective interaction t' appropriate to inelastic scattering is stronger than that within the elastic $t(q,\rho)$ produced by nuclear matter theories due to a rearrangement factor of the form

$$t'=(1+\rho\partial/\partial\rho)t . \tag{7}$$

We have found at several energies between 100 and 500 MeV that this factor is essential to a consistent description of elastic and inelastic scattering with either theoretical or empirical effective interactions. Therefore, this factor is employed in the present analysis also.

B. Effective interactions

Following Hüfner and Mahaux,[28] two calculations of the Brueckner G matrix for an energetic nucleon propagating through nuclear matter have been performed for energies near 300 MeV.[6,7] Both include similar Pauli blocking and self-energy corrections, but use rather different prescriptions for reducing nonlocal nuclear-matter results to local pseudopotentials amenable to scattering calculations. First, the Hamburg group[6] used the Paris potential[29] to evaluate the G matrix and then constructed an effective interaction according to the generalization of the Siemens averaging prescription[30] developed by Brieva and Rook.[5] Hence, this interaction, which we designate PH, includes off-shell information via short-range correlations carried by the pair wave function. Next, Nakayama and Love[7] (NL) developed an alternative prescription for reducing the G matrix to pseudopotential form that is designed to reproduce on-shell matrix elements of a nuclear-matter calculation. This method was applied using the Bonn potential.[31] Although these calculations use different nucleon-nucleon potentials, the differences between the resulting effective interactions appear to be too large to attribute to the differences between the potentials alone and are probably due to ambiguities in the reduction procedure.

Alternatively, Ray[8] developed a method for evaluating medium modifications to the Watson optical model[32] for

energies above pion threshold based upon a coupled-channels nucleon-isobar model. This method also includes Pauli blocking and includes binding potentials for intermediate nucleon and isobar states, but, unlike the Brueckner models, does not include the projectile optical potential in the energy denominator. Nevertheless, the energy dependence of the binding potential results in a repulsive contribution to the real central component of the effective interaction that is similar to earlier G-matrix calculations. The effect of isobar coupling is much smaller.

Each of these interactions can be represented by the parametrization[2,3]

$$t_i(q,\kappa)=(S_i-d_i\kappa^{\alpha_i})t_i^f(q,0) +\kappa^{\gamma_i}q^{\delta_i}\sum_n a_{in}[1+(q/\mu_{in})^2]^{-\beta_i} , \quad (8)$$

where $\kappa=k_F/1.33$ represents the local Fermi momentum relative to saturation density and where t_i^f represents the ith component of the free interaction at zero density. The scale factors S_i are normally fixed to unity for theoretical interactions but may be allowed to vary in phenomenological analyses of scattering data. The q dependence is based upon the Yukawa expansion of the t matrix, for which the exponent β assumes the values 1 for central, 2 for spin orbit (τ^{LS}), and 3 for tensor components. Similarly, $\delta=2$ for tensor interactions and $\delta=0$ otherwise. The damping factor d_i is most useful for the imaginary part of the central interaction, for which the Clementel-Villi model[9] predicts $\alpha=2$ and $d\propto E^{-1}$. Similarly, the density dependence of real parts of the effective interaction is usually assumed to be proportional to density, so that $\gamma=3$.

The free interaction $t(q,0)$ used in Eq. (8) for the PH and NL effective interactions is obtained by extrapolation to zero density. A different procedure is used for the Ray interaction. In that calculation, medium modifications were calculated using the Lomon and Feshbach model[33] and then, before performing scattering calculations, the difference between density-dependent and density-independent interactions was added to a t-matrix constructed from the Arndt phase shifts.[16] Hence, the theoretical t matrix was replaced by a phenomenological t matrix. Therefore, we fitted the Ray interaction using Eq. (8) and the original low-density limit and then replaced $t(q,0)$ with the Franey-Love (FL) t matrix. This procedure reproduces the interactions of Ref. 8 quite closely.

Unfortunately, these three free interactions are rather discordant. The isoscalar spin-independent central and spin-orbit components of the PH, NL, and FL t matrices are compared in Fig. 2. It is also instructive to compare the quantities

$$|t_m|^2=|t^C|^2+|t^{LS}|^2 , \quad (9a)$$

$$A_y=\frac{2\,\mathrm{Im}t^C t^{LS*}}{|t^C|^2+|t^{LS}|^2} , \quad (9b)$$

because, in the plane-wave approximation, the cross section is proportional to $|t_m|^2$ and the analyzing power is equal to this A_y. The disturbingly large variations shown in Fig. 3 for these quantities will translate into ambiguities in the NRIA calculations based upon these interactions. Most notably, the interaction strength is much lower for the NL interaction than for the PH and FL interactions, probably because the NL calculation extrapolates the Bonn potential well beyond its intended energy regime. The difference between the real central components of the PH and FL t matrices at large momentum transfers was also noted at lower energies[2] and is probably due to the fact that the prescription used by the PH calculation to construct the effective interaction does not properly reduce to the t matrix at zero density. However, the discrepancy between the $\mathrm{Re}t_{00}^C$ components of these interactions is much larger at 318 MeV than it is for energies below 200 MeV.

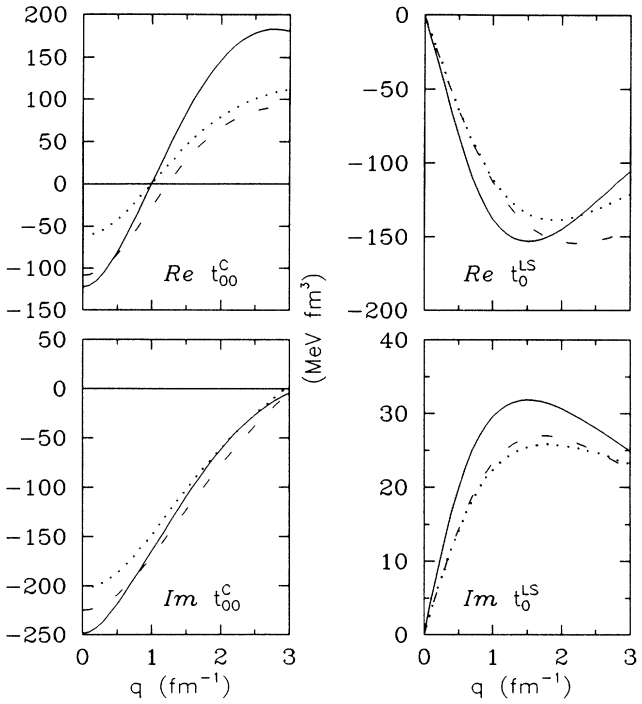

FIG. 2. Free t matrices for the PH (solid), NL (dots), and FL (dashes) interactions at 318 MeV, including knockon exchange.

The density dependence of these three models of the effective interaction is compared in Figs. 4 and 5. Parameters fitted to these interactions are collected in Table I. For all three interactions, the density dependence of $\mathrm{Re}t^C$ can be represented as a short-ranged repulsive contribution proportional to density. Although the strength of this term is similar for the PH and Ray calculations, both the free and the density-dependent terms of the NL interaction are only about half as strong. The density dependence of $\mathrm{Im}t^C$ for both NL and Ray interactions can be described by nearly pure damping and have similar strengths, but the density dependence of this component of the PH interaction is weaker and requires a significant Yukawa contribution. The density depen-

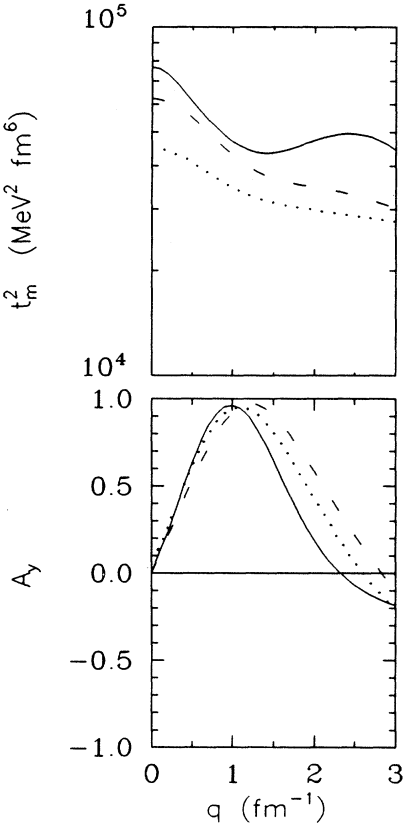

FIG. 3. Matter interaction and analyzing powers in the plane-wave approximation are shown for the PH (solid), NL (dots), and FL (dashes) interactions.

dence of the spin-orbit interaction is of similar strength for all three interactions, but the sign of the density-dependent contribution to $\mathrm{Im}\tau^{LS}$ for the NL interaction is opposite that of the others.

Therefore, all three calculations predict that medium modifications to the effective interaction remain important at 318 MeV. However, it is clear from the lack of consensus among the theories that a phenomenological analysis of density dependence will be needed for a quantitative description of the effective interaction useful to nuclear structure applications, such as extraction of neutron transition densities.[34] For this purpose we use the simpler parametrization[3]

$$\mathrm{Re}t^C(q,\kappa)=S_1\mathrm{Re}t^C(q,0)+b_1\kappa^3[1+(q/\mu_1)^2]^{-1}\ , \quad (10a)$$

$$\mathrm{Im}t^C(q,\kappa)=(S_2-d_2\kappa^2)\mathrm{Im}t^C(q,0)\ , \quad (10b)$$

$$\mathrm{Re}\tau^{LS}(q,\kappa)=S_3\mathrm{Re}\tau^{LS}(q,0)+b_3\kappa^3[1+(q/\mu_3)^2]^{-2}\ , \quad (10c)$$

containing six free parameters (S_1, b_1, S_2, d_2, S_3, and b_3). The mass parameters $\mu_1=2.0$ fm^{-1} and $\mu_3=6.0$ fm^{-1} were chosen to give a good description of the Ray interaction at 320 MeV.

Although the PH interaction gives the best available theoretical description of both elastic- and inelastic-

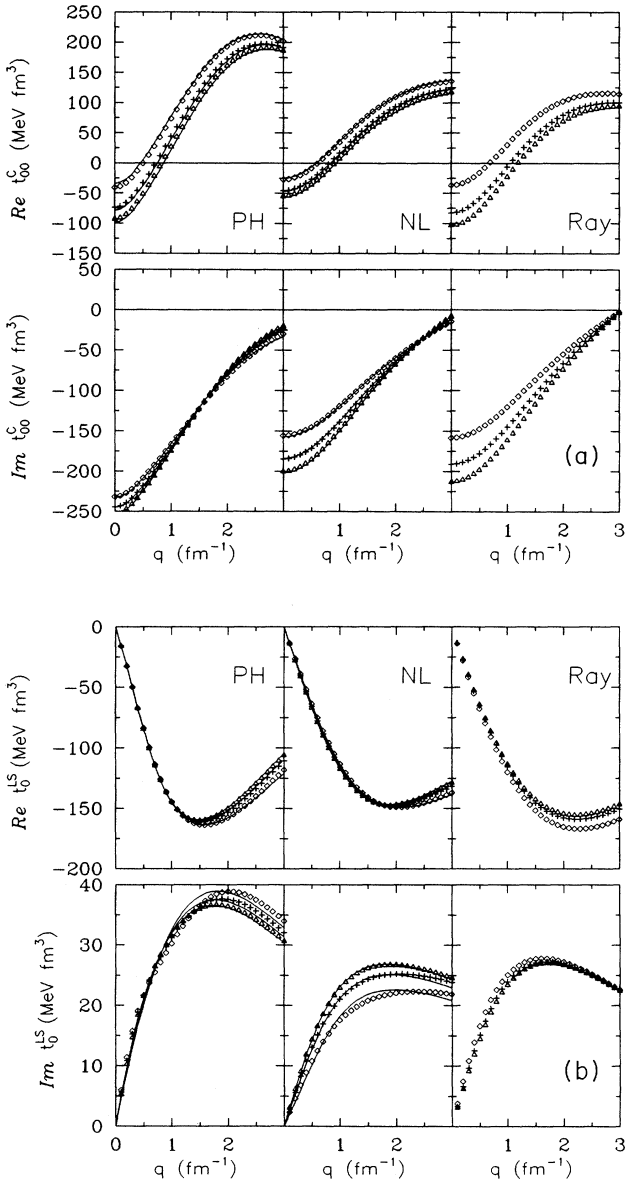

FIG. 4. (a) Central components of the PH, NL, and Ray effective interactions. The symbols show these interactions for $k_F=0.6$ (triangles), 1.0 (crosses), and 1.4 fm^{-1} (diamonds). In each panel the curves show two parameter fits to the density and momentum-transfer dependence of medium modifications to each of the interactions. No fit is shown for the Ray interaction because the reparametrized interaction after replacement of the free interaction is displayed. (b) Spin-orbit components of the PH, NL, and Ray effective interactions are displayed along with fits to the medium modifications, using the same legend as (a).

scattering data for energies below 200 MeV, and will be seen in the following section to also describe proton scattering at 318 MeV relatively well, we choose to base phenomenological analyses of these data upon the FL interaction instead for several reasons. First, the Paris po-

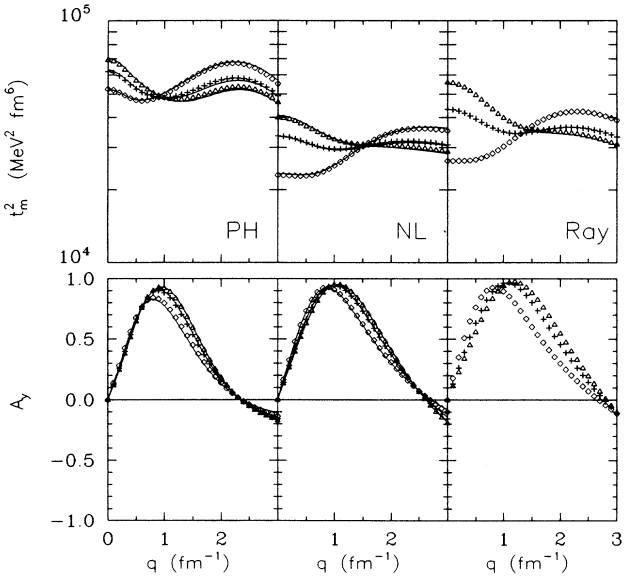

FIG. 5. Matter interactions and analyzing powers in plane-wave approximation are shown for the PH, NL, and Ray interactions for three densities: $k_F=0.6$ (triangles), 1.0 (crosses), and 1.4 fm^{-1} (diamonds).

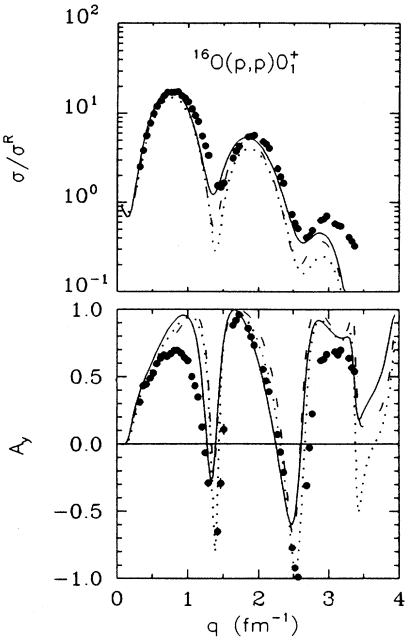

FIG. 6. Elastic-scattering calculations for $p+^{16}O$ at 318 MeV in the impulse approximation are compared with the present data. The cross section is shown as ratio to Rutherford (σ^R) to enhance detail. Solid lines are based upon the PH interaction, dots upon NL, and dashes upon FL.

tential is not strictly applicable to energies above pion threshold. Second, the difference between the FL interaction and the PH interaction for zero density is too large at 318 MeV. This discrepancy may be due to the fact that the method used to evaluate the effective interaction involves a ratio between correlated and uncorrelated matrix elements for which the denominator is small near 300 MeV and may amplify defects of the model.[35] Third, fits using the PH interaction for t^f tend to be unstable but generally produce small values for S_1 which have the effect of suppressing $\mathrm{Re}t_{00}^C$ at high q anyway. Fourth, fits based upon the FL interaction were found to be much more stable and to produce scale factors closer to unity. Finally, the FL interaction should provide a better model of the free interaction and is applicable to higher energies. Therefore, we use the FL t matrix for t^f and model the medium corrections upon the Ray interaction for energies above 300 MeV.

IV. RESULTS

A. Impulse approximation

In this section we compare the data for elastic scattering and for three of the strongest inelastic transitions

TABLE I. Reparametrization of theoretical effective interactions.

Component	α[a]	μ[b]	Coefficients	PH	NL	Ray
$\mathrm{Re}t_{00}^C$	3	0	a_{11} (MeV fm^3)	−24.05	9.73	0
	3	3.0 fm^{-1}	a_{12} (MeV fm^3)	83.22	18.53	0
	3	2.0 fm^{-1}	a_{13} (MeV fm^3)	0	0	61.19
$\mathrm{Im}t_{00}^C$	2		d_2	0.151	0.280	0.267
	2	0	a_{21} (MeV fm^3)	−15.87	−9.46	0
$\mathrm{Re}\tau_0^{LS}$	3	3.0 fm^{-1}	a_{31} (MeV fm^5)	−4.05	−5.00	0
	3	6.0 fm^{-1}	a_{32} (MeV fm^5)	3.70	3.45	1.74
$\mathrm{Im}\tau_0^{LS}$	2		d_4	−0.119	0.135	0
	2	1.0 fm^{-1}	a_{41} (MeV fm^5)	2.70	1.85	0
	3	1.0 fm^{-1}	a_{42} (MeV fm^5)	0	0	−1.55

[a] The density dependence of each term is proportional to κ^α and we set $\gamma=\alpha$ for simplicity. Note that $\delta=0$ throughout and $\beta=1$ for central and $\beta=2$ for spin-orbit components.

[b] An entry of 0 is to be interpreted as a delta function with $\mu^{-1}=0$.

with NRIA calculations based upon the PH and NL interactions at zero density with corresponding results for the FL t matrix. Elastic-scattering results are shown in Fig. 6 and inelastic-scattering results for selected states of ^{16}O are shown in Fig. 7. The optical potentials for each of these interactions are compared in Fig. 8. Each set of inelastic calculations employs consistent distorted waves based upon the NRIA optical potential produced by the same effective interaction used for the transition potential.

Elastic-scattering cross sections are presented as ratios to the point-charge Rutherford cross section (σ^R) to enhance detail. We find that better agreement with the data would be obtained if the diffractive patterns for all three interactions could be shifted towards larger momentum transfer. This comparison suggests that a short-ranged repulsive contribution to the effective interaction might be beneficial. For small momentum transfers, the predicted analyzing powers are substantially larger than observed in the data. Recognizing that $\mathrm{Im}t^C \gg \mathrm{Re}t^{LS}$ for low q, the structure of Eq. (9b) suggests that these analyzing powers could be suppressed either by enhancing $\mathrm{Im}t^C$ or by suppressing $\mathrm{Re}t^{LS}$.

Although the three t matrices appear to differ considerably, Figs. 6–8 show that effects upon distorting and scattering potentials tend to compensate when consistent

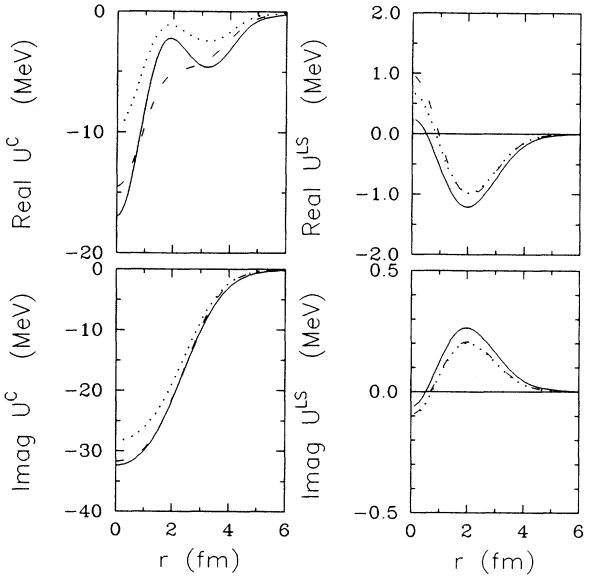

FIG. 8. Optical potentials for $p + ^{16}$O at 318 MeV in the impulse approximation are shown for the PH (solid), NL (dots), and FL (dashes) interactions.

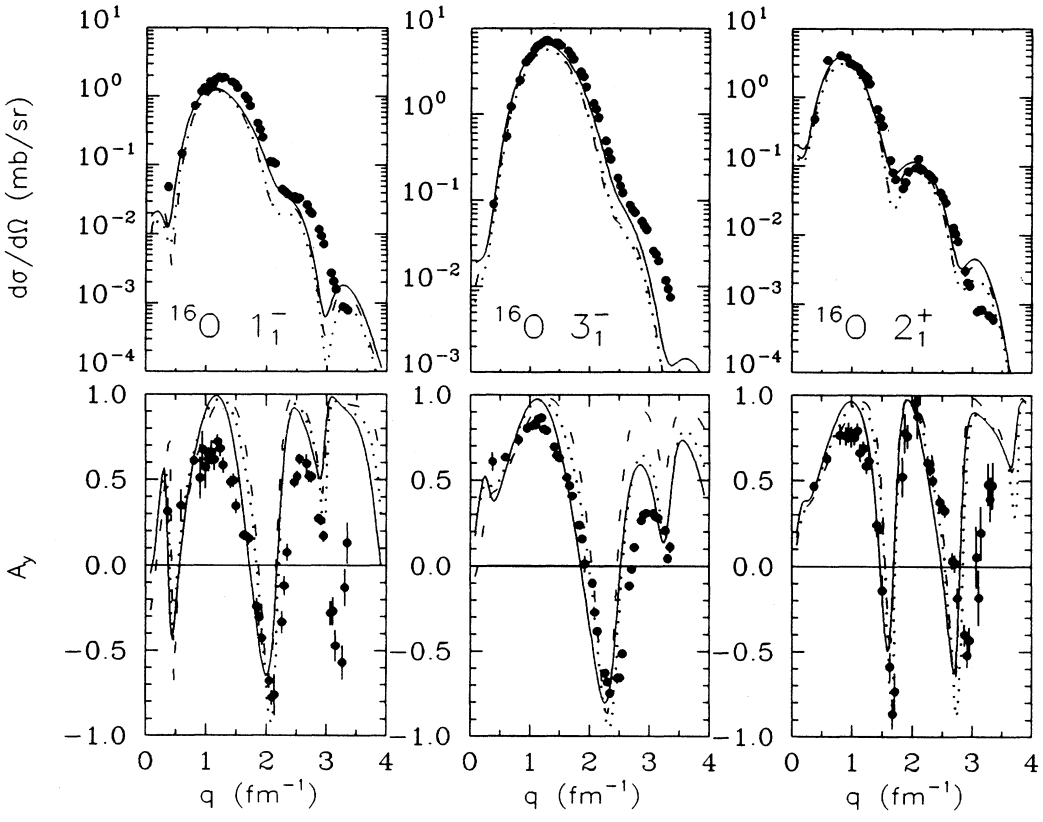

FIG. 7. Impulse-approximation calculations based upon the PH (solid), NL (dots), and FL (dashes) interactions are compared with the present 318-MeV data for the 1_1^-, 3_1^-, and 2_1^+ states of ^{16}O.

distorted waves are employed. The imaginary part of the central interaction dominates the inelastic cross section and the optical potential for this energy. Although the relative weakness of this component of the NL interaction might suggest that the cross sections calculated using this interaction would be much smaller than calculated using the other interactions, the absorptive potential is also weaker. This effect can be seen in the $\mathrm{Im}U^C$ curves in Fig. 8. Apparently the enhanced flux compensates for the reduced transition strength so that inelastic cross sections for all three interactions remain similar in the impulse approximation.

The NRIA calculations are most accurate for the 2_1^+ state, for which the transition density peaks at the largest radius,[24] and are least accurate for the 1^- state, for which the transition density has a strong interior lobe. The transition density for the 3^- state peaks at an intermediate radius and the impulse approximation achieves intermediate quality. For momentum transfers larger than about 1.5 fm^{-1}, the 3^- calculations would be improved by a repulsive contribution to the interaction that shifts the angular distributions outward. This effect is reminiscent of similar effects for lower projectile energies[1-4] and can be attributed to the density dependence of the real part of the central interaction. However, whereas NRIA calculations for the 1_1^- state produce cross sections for energies below 200 MeV that are considerably larger than the data for low momentum transfers,[1-4] the NRIA calculations for 318 MeV are below the data for all $q < 3$ fm^{-1}.

B. Local-density approximation

LDA calculations of optical potentials based upon the PH, NL, and Ray interactions are compared in Fig. 9.

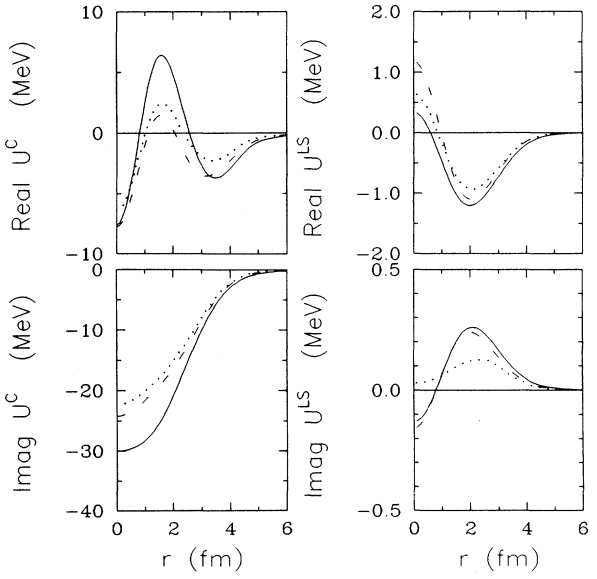

FIG. 9. Optical potentials for $p + {}^{16}O$ at 318 MeV in the local-density approximation are shown for the PH (solid), NL (dots), and Ray (dashes) interactions.

Upon comparison between Figs. 8 and 9, we observe that the largest effects due to density dependence are to be found in the central potentials. Pauli blocking suppresses the absorptive potential with little change in shape, whereas the short-range repulsive contribution to $\mathrm{Re}t^C$ sharpens the interior structure of the real potential.

LDA calculations for elastic scattering are compared with the data in Fig. 10. The enhanced repulsion in $\mathrm{Re}t^C$ pushes the angular distributions outward and thereby improves the description of the data. However, the damping of $\mathrm{Im}U^C$ predicted by the NL and Ray interactions results in a reduction of the cross section that is too large. This effect is smaller for the PH interaction, which therefore gives a much better description of the cross-section data. Note that structure near 3 fm^{-1} is probably due to a third peak in the elastic form factor and is described better when the density of Ref. 26 is used instead of the smoother density of Ref. 25.

Therefore, of the available theories of the effective interaction, the PH model continues at this energy to give the best fit to elastic-scattering data as also found for lower energies.[2,4] However, even this model overpredicts the forward-angle analyzing power. This problem, characteristic of the NRIA for $E_p = 300-800$ MeV, remains even after Pauli blocking and dispersion corrections to the effective interaction are applied.[8]

Inelastic-scattering calculations for the 1_1^-, 2_1^+, and 3_1^- states are compared with the data in Fig. 11. All of the calculations employ self-consistent distorted waves and transition densities from electron-scattering measure-

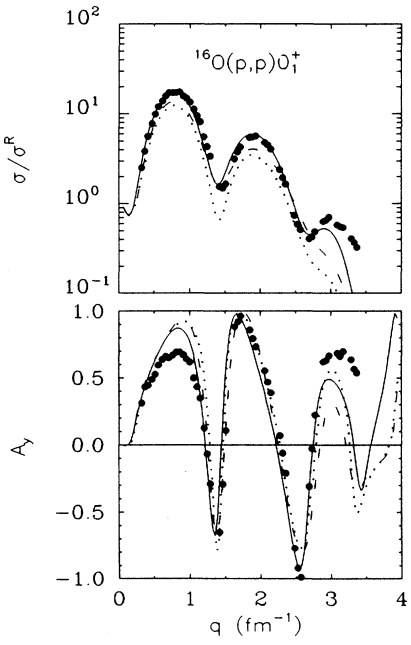

FIG. 10. Elastic-scattering calculations for $p + {}^{16}O$ at 318 MeV in the local-density approximation are compared with data. Solid lines are based upon the PH, dots upon the NL, and dashes upon the Ray interactions.

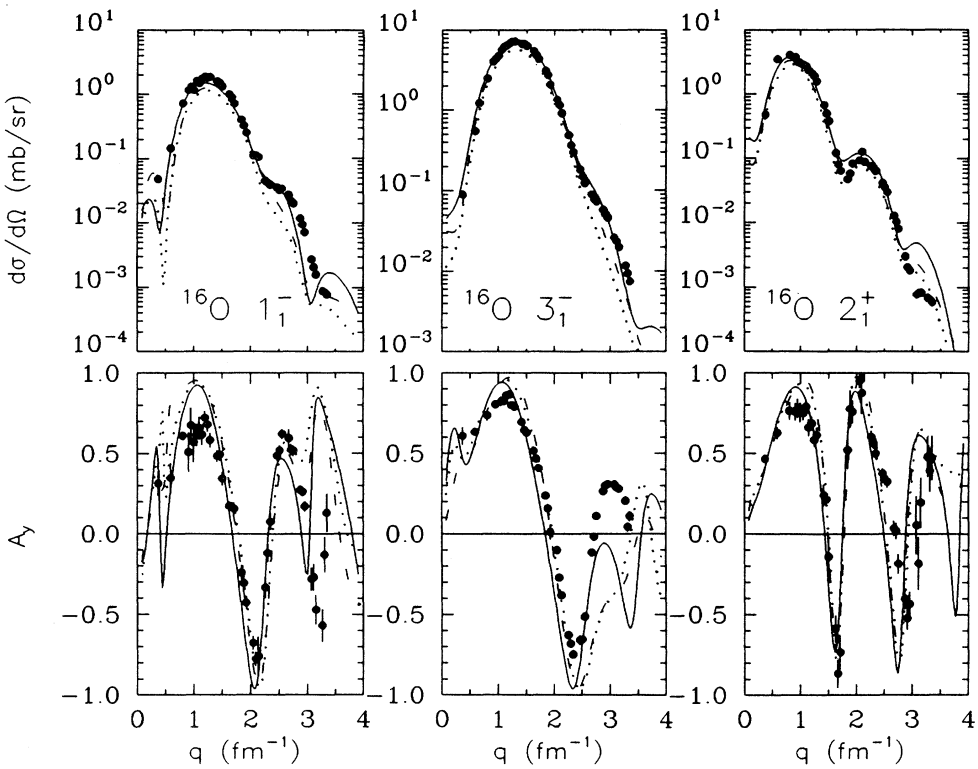

FIG. 11. LDA calculations based upon the PH (solid), NL (dots), and Ray (dashes) interactions are compared with 318-MeV data for the 1^-_1, 3^-_1, and 2^+_1 states of ^{16}O.

ments. Density-dependent corrections to the PH and Ray interactions produce modest improvements in both the elastic- and the inelastic-scattering calculations, with the improvements being somewhat larger for the PH interaction. Most notably, the cross sections are shifted outwards and the low-q analyzing powers are reduced to some degree, but the effects are not large enough to obtain precise quantitative agreement with the data.

Although medium modifications to the NL interaction severely reduce the elastic cross section, the effect upon inelastic scattering is mitigated by the use of consistent distorted waves. Hence, modest improvements in the inelastic-scattering calculations can be obtained for the NL interaction despite its failure for elastic scattering. Although the NL prescription may be superior to the PH interaction for tensor and spin-flip components,[7] it is no better at this energy for normal-parity isoscalar excitations than at lower energies for which similar difficulties have already been reported.[2,4]

LDA calculations for the other normal-parity isoscalar states observed in this experiment are compared with the data in Figs. 12 and 13. The calculations are extended to 3 or 4 fm^{-1} even though electron-scattering measurements for these states only determine the form factors to about 2.7 fm^{-1}. Hence, some of the oscillations for large momentum transfers are simply artifacts of limitations in the electroexcitation data.

LDA calculations based upon the PH interaction are in good agreement with the data for most states. Both the cross section and the analyzing power for the 2^+_3 and 4^+_1 states are well described by the calculation. The cross-section calculation for the 0^+_3 state is more successful at 318 MeV than for energies below 200 MeV (Refs. 2–4) presumably because the spin-convection contribution[36] neglected by these calculations is relatively small at this energy due to the increasing dominance of the central interaction over the spin orbit. We also observe that the 2^+_2 calculations are also more accurate, suggesting that the $0^+_1 \rightarrow 2^+_1 \rightarrow 2^+_2$ two-step contribution is relatively smaller at this energy. Finally, we note that, much like the situation at lower energies, the unresolved 3^+_1 state contaminates the 4^+_2 data, enhancing the cross section for large momentum transfer and producing an analyzing power uncharacteristic of direct normal-parity isoscalar excitations.

In conclusion, the data clearly indicate that density-dependent contributions to the effective interaction remain important near 300 MeV, but the theoretical calculations presently available provide only modest improvements over the impulse approximation. Therefore, it is appropriate to extend the empirical interaction into this energy regime.

C. Empirical effective interaction

We have analyzed the inelastic-scattering data using the methods developed and previously applied in Refs. 3 and 4. Six parameters of the empirical effective interac-

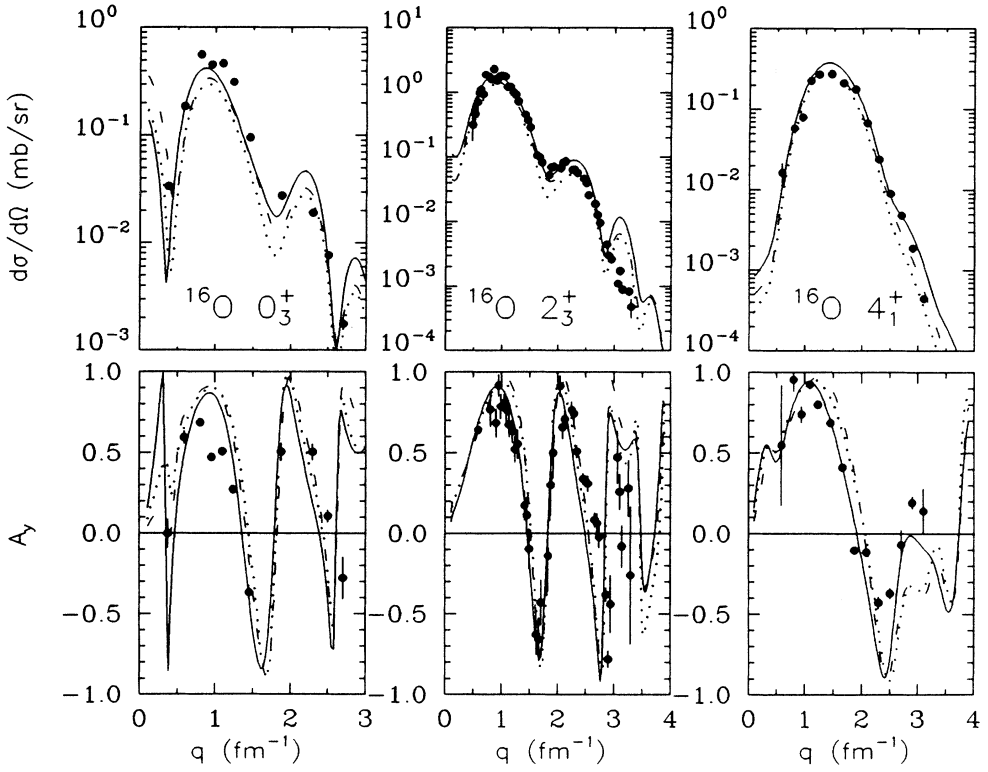

FIG. 12. LDA calculations based upon the PH (solid), NL (dots), and Ray (dashes) interactions are compared with data for the 0_3^+, 2_3^+, and 4_1^+ states of ^{16}O.

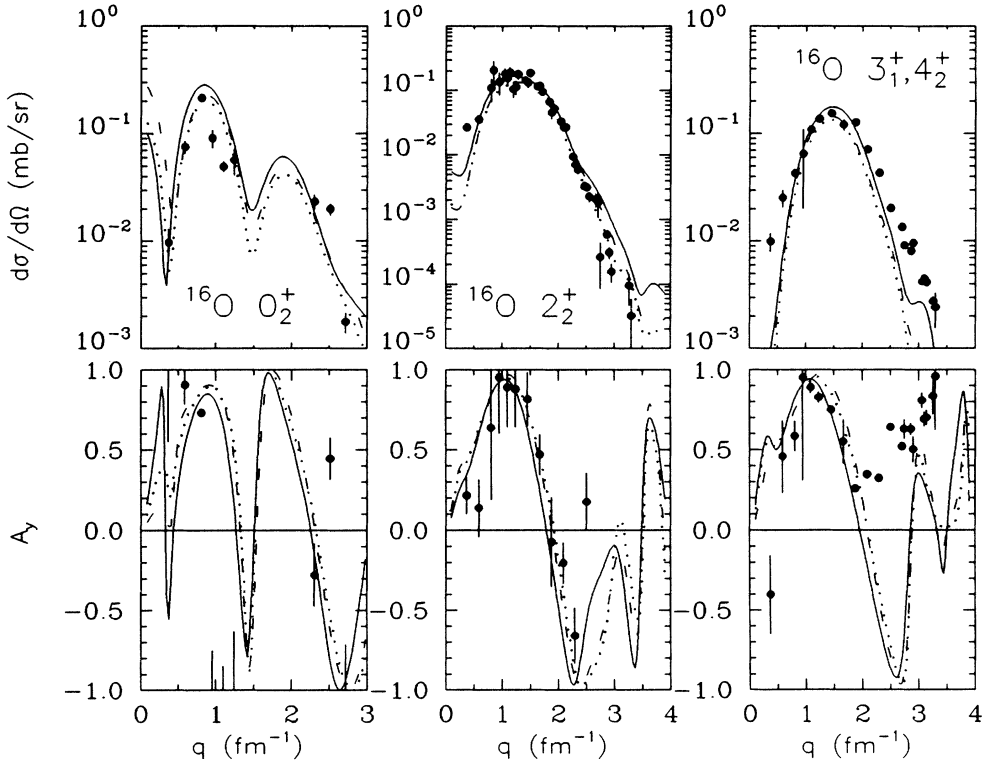

FIG. 13. LDA calculations based upon the PH (solid), NL (dots), and Ray (dashes) interactions are compared with data for the 0_2^+, 2_2^+, and 4_2^+ states of ^{16}O. Note that a 3^+ state remains unresolved from the 4_2^+ data.

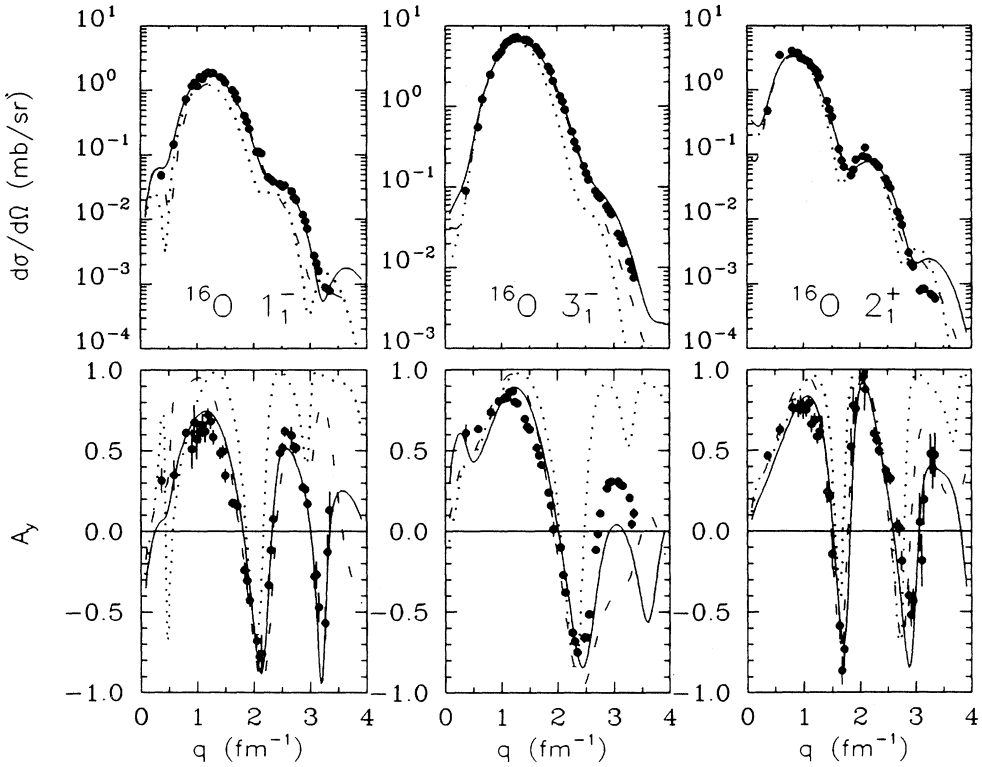

FIG. 14. Fits based upon the empirical effective interaction are shown as solid lines and compared with data for the 1^-_1, 3^-_1, and 2^+_1 states of ^{16}O at 318 MeV. Note that data for $q > 2.7$ fm^{-1} were not included in the fitting procedure. Also shown are IA results (dots) based upon the FL interaction and LDA results (dashes) based upon the Ray interaction.

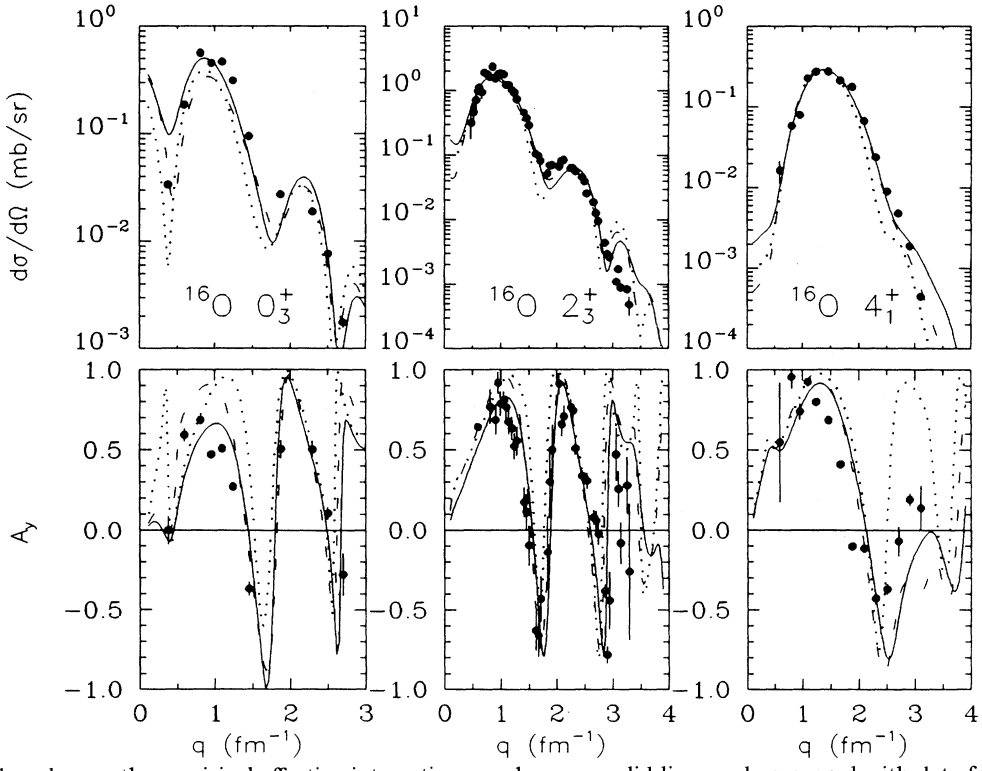

FIG. 15. Fits based upon the empirical effective interaction are shown as solid lines and compared with data for the 0^+_3, 2^+_3, and 4^+_1 states of ^{16}O at 318 MeV. Note that data for the 0^+_3 state were excluded from the fitting procedure. Also shown are IA results (dots) based upon the FL interaction and LDA results based upon the Ray interaction.

tion were fitted to the cross-section and analyzing power data for five states of ^{16}O simultaneously, including the 1_1^-, 2_1^+, 2_3^+, 3_1^-, and 4_1^+ states. These are the states for which the reaction mechanism and nuclear structure are known best. The transition density for the 1_1^- state is peaked in the interior and is thus most sensitive to the high-density properties of the effective interaction.

Although Figs. 14 and 15 display the full angular range spanned by the experiment, the fit was limited to momentum transfers $q \leq 2.7$ fm^{-1} for which the transition densities are known accurately from electroexcitation measurements. We also show the 0_3^+ state, which has good interior sensitivity, even though it was excluded from the fit. Additional uncertainties of $\pm 5\%$ for cross sections and ± 0.05 for analyzing powers were folded into the experimental error bars to smooth the relative weights assigned to various states and momentum transfers.

The empirical interaction was modeled upon the Ray interaction. The FL t matrix was used for the free interaction $t(q,0)$ and the masses $\mu_1=2.0$ fm^{-1} and $\mu_3=6.0$ fm^{-1} which gave good fits to the Ray interaction were used. The analysis began using the parameters listed in Table I for the Ray interaction as initial estimates for the empirical interaction. The density dependence of the imaginary spin-orbit interaction is not strong enough to fit and was held fixed. The six free parameters were fitted to the inelastic-scattering data using a self-consistency cycle in which distorted waves for a given interaction were based upon the average of the parameters produced by the preceding two interactions.[3,4]

The fit to the data is compared with the results of the free interaction and the Ray effective interaction in Figs. 14 and 15. The empirical effective interaction provides a much better fit to the 1_1^- and 3_1^- cross-section data and to the low-q analyzing powers for all of the states. The changes observed for states with surface-peaked densities are somewhat smaller than for interior densities but the fitted interaction always produces at least some improvement in the calculated analyzing powers and high-q cross sections. Thus, we find that an effective interaction which depends upon local density is capable of consistently describing inelastic-scattering data for many states of a given target simultaneously. Furthermore, we have found that the same interaction gives an excellent description of inelastic scattering for ^{40}Ca and that when both sets of data are included in a global analysis essentially the same parameters emerge.[37] Therefore, the LDA appears to apply very well to the scattering of 318-MeV protons.

Elastic-scattering calculations are compared with the data in Fig. 16. Although these data were not included in the analysis, the analyzing power prediction is nonetheless improved, particularly at low momentum transfers.

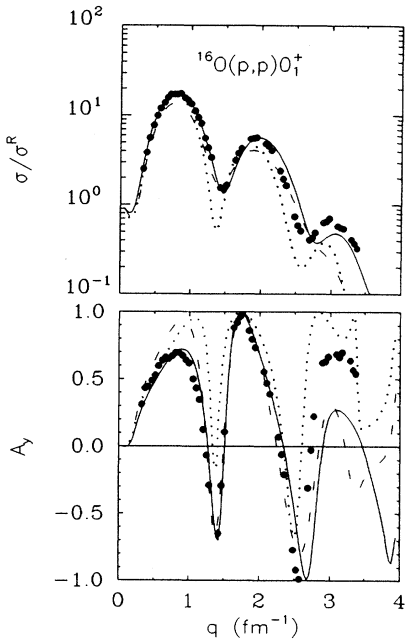

FIG. 16. Elastic-scattering calculations for $p+^{16}O$ at 318 MeV based upon the empirical interaction fitted to inelastic-scattering data are shown as solid lines. Note that the elastic data were not included in the fitting procedure. Nevertheless, the results are superior to the IA (dots) and to the LDA (dashes) based upon the Ray interaction.

The elastic cross section is improved near 1.2 fm^{-1}, but the outward shift at larger q appears to be somewhat too large. However, discrepancies for larger momentum transfer may be attributed to deficiencies in the ground-state density fitted to electron-scattering data that are limited to $q \leq 3.0$ fm^{-1}. Similar improvements of elastic-scattering calculations for ^{40}Ca are also obtained with the empirical effective interaction.[37]

The parameters of the empirical effective interaction are compared with initial estimates based upon the Ray interaction in Table II. The central and spin-orbit components of the empirical interaction are plotted in Fig. 17 and should be compared with the theoretical interactions plotted in Figs. 4 and 5. We find that the density dependence of the real central interaction is stronger at low q for the empirical interaction than for any of the theoretical interactions, but that the strength at high q is intermediate between the PH and Ray interactions. The density dependence of Imt^C is smaller than predicted and of opposite sign, such that absorption appears to increase slightly with density rather than being damped according

TABLE II. Comparison of empirical effective interaction with predictions of the Ray model.

Interaction	S_1	b_1 (MeV fm^3)	S_2	d_2	S_3	b_3 (MeV fm^5)
Ray	1.0	61.2	1.0	0.267	0	1.74
Empirical	1.068	144.7	1.021	−0.067	0.833	7.14

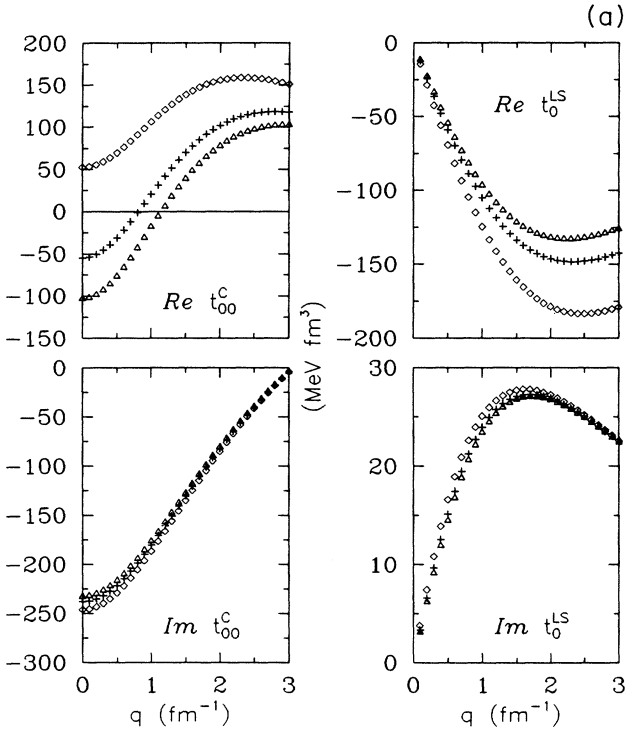

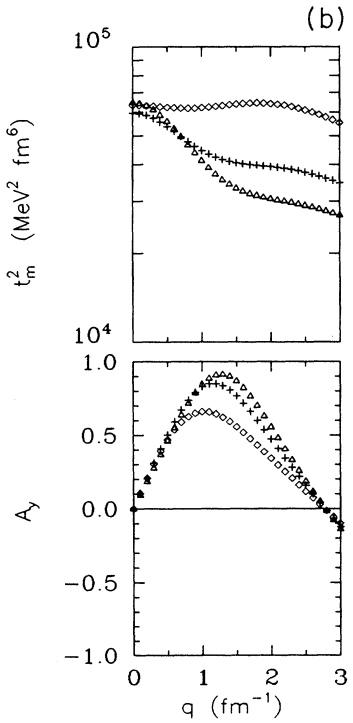

FIG. 17. (a) Central and spin-orbit components of the empirical interaction are shown for three densities: $k_F=0.6$ (triangles), 1.0 (crosses), and 1.4 fm^{-1} (diamonds). (b) Matter interactions and analyzing powers in the plane-wave approximation are shown for the empirical interaction at three densities: $k_F=0.6$ (triangles), 1.0 (crosses), and 1.4 fm^{-1} (diamonds).

to estimates based upon Pauli blocking. Note that the central scale factors S_1 and S_2 are slightly larger than unity at this energy, but that $S_3=0.83$ remains consistent with results for lower energies for which all three scale factors tend to near 0.8. On the other hand, the density dependence of Ret^{LS} is substantially stronger for the empirical interaction than for any of the theories shown in Fig. 4.

The uniqueness of these results was studied by using a grid search in which each of the six parameters was stepped along a specified grid of values. For each grid point, the remaining five parameters were fitted using the customary self-consistency cycle. No alternative solution was found. In particular, the grid confirms the values found for b_1, d_2, and S_3 as essential features of the effective interaction for proton inelastic scattering at 318 MeV. However, the unusually large density dependence found for Ret^{LS} at this energy may not be firmly established because the χ^2 surface is soft with respect to b_3. Nevertheless, similar values for b_3 are also obtained at 500 MeV (Ref. 14) and for ^{40}Ca$(\vec{p},p')$ at 318 MeV.[37]

Ambiguities in the choice of mass parameters μ_i and the weighting of data sets were found to produce only unimportant variations in the precise values of the fitted parameters while leaving the essential features of the interaction unaffected. For example, if we supplement the damping factor used in Eq. (10b) with a Yukawa contribution so that

$$\mathrm{Im}t^{C}(q,\kappa)=(S_2-d_2\kappa^2)\mathrm{Im}t^{C}(q,0)+b_2\kappa^2[1+(q/\mu_2)^2]^{-1} \tag{11}$$

with $\mu_2=2.0$ fm^{-1}, we can find an equivalent fit to the data which produces essentially the same interaction plotted in Fig. 17 using $d_2=0$ and a negative value of b_2. Alternatively, the damping parameter d_2 could be constrained to nuclear matter estimates of Pauli blocking provided that b_2 becomes even more negative. For example, if $d_2=0.267$ is held fixed to the value extracted from the Ray interaction, then a fit based upon Eq. (11) yields $b_2=-67$ MeV fm^3 with insignificant changes in the remaining parameters. The resulting interaction is practically indistinguishable from Fig. 17. Similar results are also found at 500 MeV.[14] Therefore, we can interpret the anomalous negative result for d_2 as an indication that a new absorption mechanism strong enough to mask the Pauli blocking effect operates at energies above 300 MeV.

We have also attempted to fit the data using the PH model for the free interaction. Unlike the analyses made for energies below 200 MeV, where better fits are obtained using the PH instead of the FL t matrix, at this energy we find that fits based upon the PH interaction tend to be unstable and are definitely inferior to fits based upon the FL t matrix. Although such fits tend to give smaller values of b_1, the real central scale factor S_1 is usually less than 0.5. Evidently, the fitting procedure uses S_1 to suppress Ret^{C} for zero density because it is unrealistically strong at high momentum transfer. However, fits using either free interaction produce similar interactions for higher densities even though the parame-

ters differ. Hence, we believe that the essential characteristics of the empirical effective interaction are well determined despite possible ambiguities in the best choice of free interactions and other details of the model.

Therefore, the density dependence of the effective interaction fitted to inelastic-scattering data for 318-MeV protons is substantially stronger than predicted by nonrelativistic theories of nuclear matter. The real central interaction contains a strong short-range repulsive contribution proportional to density, whereas damping of the imaginary central interaction due to Pauli blocking appears to be absent or even reversed. If we assume that Pauli blocking continues to follow the E^{-1} trend from lower energies, this result might suggest that a new absorption mechanism occurs for energies above pion threshold that is strong enough to mask the expected damping effect. Similar results are also found at 500 MeV. Yet, below 200 MeV, the density dependence of the empirical interaction is somewhat less than predicted by nuclear-matter theory. Further investigations will be needed to clarify the qualitative change in medium modifications of the proton-nucleus effective interaction that appears to occur near 300 MeV.

D. Comparison with IA2

Ottenstein *et al.*[12] have performed a systematic analysis of elastic-scattering results for the RIA using a meson-exchange model designated IA2. It has been suggested that the principal difference between relativistic and nonrelativistic versions of the impulse approximation should be identified with the contribution of virtual $N\bar{N}$ pairs in the medium.[38] When reduced to Schrödinger form, the contribution of virtual $N\bar{N}$ pairs amounts to an effective density dependence which can be described as primarily a short-ranged interaction.[12]

The Schrödinger-equivalent IA2 optical potentials are compared with the present results in Fig. 18. The pair contributions to the spin-orbit and the imaginary central potentials are quite modest and these potentials agree well with the phenomenological results. The agreement for the imaginary central potential, which dominates the cross section and which is significantly larger than the LDA predictions of Fig. 9, is particularly impressive. Also, note that the spin-orbit potential is not especially influential for small radii.

The pair contribution to the real central potential, on the other hand, is strong and positive. This contribution is strongest in the interior where the density is large and becomes small in the surface. The net result is very similar to the PH potential shown in Fig. 9. The empirical result is similar in shape but boasts a somewhat stronger repulsive density dependence.

Elastic-scattering calculations based upon these IA2 potentials are compared with the data in Fig. 19. The agreement with the data is slightly better than we obtained with the interaction fitted to inelastic scattering. However, a direct comparison cannot actually be made because the IA2 calculations used the Dirac-Hartree wave functions of Horowitz and Serot[39] rather than the experimental density we used. Nevertheless, the fact that our elastic calculations appear to contain slightly too much repulsion suggests that the best fit to the data would be obtained with a real central potential closer to the IA2 result.

At lower energies, such as 200 MeV, the IA2 model

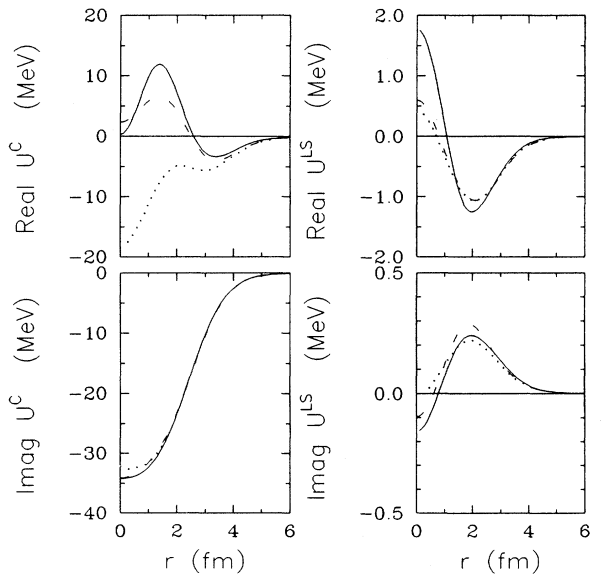

FIG. 18. Optical potentials based upon the empirical interaction (solid) are compared with complete (dashes) and "no-pairs" (dots) Schrödinger-equivalent potentials from the IA2 model.

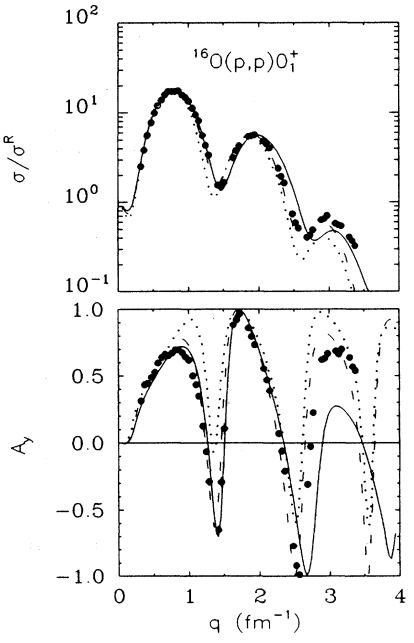

FIG. 19. Elastic-scattering calculations based upon the IA2 potentials (dashes) are compared with 318-MeV data for ^{16}O and with calculations based upon the empirical interaction fitted to inelastic-scattering data (solid).

does not describe elastic-scattering data this well—it tends to produce cross sections that are too large and analyzing powers without adequate oscillation amplitude.[12] These deficiencies can be reduced by applying an *ad hoc* Pauli blocking factor[40] to the imaginary central potential motivated by the Clementel-Villi model. At 200 MeV we find that the empirical effective interaction fitted to inelastic-scattering data produces a real central potential that is similar to the IA2 prediction, but that the imaginary potential is damped.[37]

V. CONCLUSIONS

We have obtained new data for the scattering of 318-MeV protons by ^{16}O and find that substantial medium modifications of the central and spin-orbit interactions are required to describe normal-parity isoscalar excitations even at this energy. Although several theoretical models predict significant density dependence of similar form, none is able to consistently describe the data with enough accuracy to be useful for quantitative structure studies, such as the extraction of neutron transition densities. Nevertheless, an empirical effective interaction similar to those we employ in the 100–200-MeV regime fits the data quite well. With only six free parameters, this interaction was fitted to cross-section and analyzing power data for five states simultaneously, a total of ten angular distributions. Furthermore, the same interaction also fits elastic-scattering data and data for ^{40}Ca that were not included in the analysis.[37] Therefore, the empirical effective interaction is a function only of local density and is independent of both target and state, in agreement with the LDA hypothesis.

The empirical effective interaction differs from theoretical predictions in several significant respects. We find that the repulsive contribution to the real central interaction is considerably stronger than predicted by nonrelativistic theories of the effective interaction in nuclear matter. We also find that the damping coefficient applied to the imaginary central interaction is smaller in magnitude and of opposite sign than predicted. Hence, rather than describing damping of absorption due to Pauli blocking, the phenomenological result suggests that the absorptive interaction is enhanced for energies near 318 MeV. Furthermore, a similar analysis at 500 MeV reveals a similar effect with greater magnitude.[14] Therefore, a new absorption mechanism not present in existing theories seems to appear for energies above 300 MeV and may be associated with the pion threshold.

In addition, the density dependence of the spin-orbit interaction appears to be significantly stronger than theoretical predictions. However, we also find that the spin-orbit interaction is suppressed by a factor of about 0.8 at low density. This finding is consistent with similar results for the empirical effective interaction at lower energies but is not consistent with a strict interpretation of the local-density approximation, which would require the effective interaction to heal to the free interaction at zero density. We have speculated that the radial extent of nucleon orbitals may produce a nonlocal effect in finite nuclei that is approximated in the LDA by variations of the interaction at low density.[3,4]

The present results have also been compared with the relativistic IA2 model for elastic scattering. We find that the optical potentials that emerge from the phenomenological analysis are similar to the Schrödinger-equivalent potentials predicted by Ottenstein *et al.*[12] The virtual-pair contribution that differentiates between relativistic and nonrelativistic versions of the impulse approximation can evidently be represented by an effective density dependence similar to the present phenomenology. Most notably, virtual pairs produce a repulsive contribution to the real central interaction similar to the empirical result and larger than predicted by nonrelativistic nuclear matter calculations.

Insofar as the effective interaction for nucleon-nucleus scattering is a function only of local density, the fitted interaction subsumes Pauli blocking, dispersive, and relativistic effects. In addition, Arellano *et al.*[41] have shown that full-folding corrections can produce effects upon elastic scattering similar in magnitude to the Pauli blocking corrections estimated by nuclear-matter theory. Furthermore, it is suggested that the off-shell t matrix can be approximated by a local expression similar to the LDA model we employ. Other full-folding calculations based upon the Bonn potential appear to receive large contributions from the delta resonance;[42] these effects may also be modified in the medium and affect the comparison between empirical and theoretical effective interactions. Although the magnitude of off-shell effects has been disputed,[43] the empirical interaction would tend to absorb such effects also. A clear separation of these contributions will require relativistic full-folding calculations which include medium modifications due to Pauli blocking, dispersion, isobars, and possibly renormalization of meson effective masses.[44] The success of our empirical interaction suggests that it will be profitable to reduce such a calculation to a similar form so that theoretical predictions of the density-dependent parameters could be compared to their fitted values.

ACKNOWLEDGMENTS

We thank Dr. N. Ottenstein and Prof. S. Wallace for tables of the IA2 optical potentials and Dr. L. Ray for tables of his effective interaction. This work was supported by grants from the National Science Foundation and the Department of Energy.

[a]Present address: American University, Washington, D.C. 20016.

[b]Present address: Argonne National Laboratory, Argonne, IL 60439.

[c]Present address: Rogaland Research Institute, Ullandhang, N-4001, Stavanger, Norway.

[d]Present address: Allied-Signal, Los Angeles, CA 90504.

[e]Present address: California State University, Hayward, CA

94542.
[f]Present address: University of South Carolina, Columbia, SC 29208.
[g]Present address: College of William & Mary, Williamsburg, VA 23185.
[h]Present address: University of Washington, Seattle, WA 98195.
[i]Present address: University of Virginia, Charlottesville, VA 22901.
[j]Present address: CEBAF, Newport News, VA 23606.
[1]J. Kelly, W. Bertozzi, T. N. Buti, F. W. Hersman, C. Hyde, M. V. Hynes, B. Norum, F. N. Rad, A. D. Bacher, G. T. Emery, C. C. Foster, W. P. Jones, D. W. Miller, B. L. Berman, W. G. Love, and F. Petrovich, Phys. Rev. Lett. **45**, 2012 (1980).
[2]J. J. Kelly, W. Bertozzi, T. N. Buti, J. M. Finn, F. W. Hersman, C. E. Hyde-Wright, M. V. Hynes, M. A. Kovash, B. Murdock, B. E. Norum, B. Pugh, F. N. Rad, A. D. Bacher, G. T. Emery, C. C. Foster, W. P. Jones, D. W. Miller, B. L. Berman, W. G. Love, J. A. Carr, and F. Petrovich, Phys. Rev. C **39**, 1222 (1989).
[3]J. J. Kelly, Phys. Rev. C **39**, 2120 (1989).
[4]J. J. Kelly, J. M. Finn, W. Bertozzi, T. N. Buti, F. W. Hersman, C. Hyde-Wright, M. V. Hynes, M. A. Kovash, B. Murdock, P. Ulmer, A. D. Bacher, G. T. Emery, C. C. Foster, W. P. Jones, D. W. Miller, and B. L. Berman, Phys. Rev. C **41**, 2504 (1990); Q. Chen, J. J. Kelly, P. P. Singh, M. C. Radhakrishna, W. P. Jones, and H. Nann, *ibid.* **41**, 2514 (1990).
[5]F. A. Brieva and J. R. Rook, Nucl. Phys. **A291**, 299 (1977); **A291**, 317 (1977); **A297**, 206 (1978); **A307**, 493 (1978); H. V. von Geramb, F. A. Brieva, and J. R. Rook, in *Microscopic Optical Potentials,* edited by H. V. von Geramb (Springer-Verlag, Berlin, 1979), p. 104.
[6]H. V. von Geramb, in *The Interaction Between Medium Energy Nucleons in Nuclei (Indiana Cyclotron Facility, Bloomington, Indiana),* Proceedings of the Workshop on the Interactions Between Medium Energy Nucleons in Nuclei, AIP Conf. Proc. No. 97, edited by H. O. Meyer (AIP, New York, 1982), p. 44; L. Rikus, K. Nakano, and H. V. von Geramb, Nucl. Phys. **A414**, 413 (1984).
[7]K. Nakayama and W. G. Love, Phys. Rev. C **38**, 51 (1988).
[8]L. Ray, Phys. Rev. C **41**, 2816 (1990).
[9]E. Clementel and C. Villi, Nuovo Cimento **2**, 176 (1955).
[10]L. G. Arnold, B. C. Clark, and R. L. Mercer, Phys. Rev. C **23**, 15 (1981).
[11]J. A. McNeil, J. R. Shepard, and S. J. Wallace, Phys. Rev. Lett. **50**, 1439 (1983); J. R. Shepard, J. A. McNeil, and S. J. Wallace, *ibid.* **50**, 1444 (1983).
[12]N. Ottenstein, S. J. Wallace, and J. A. Tjon, Phys. Rev. C **38**, 2272 (1988); **38**, 2289 (1988).
[13]S. Hama, B. C. Clark, E. D. Cooper, H. S. Sherif, and R. L. Mercer, Phys. Rev. C **41**, 2737 (1990).
[14]B. S. Flanders, J. J. Kelly, D. Lopiano, B. Aas, A. Azizi, G. Igo, G. Weston, C. Whitten, A. Wong, M. V. Hynes, J. McClelland, W. Bertozzi, J. M. Finn, C. E. Hyde-Wright, R. W. Lourie, B. E. Norum, P. Ulmer, and B. L. Berman, Phys. Rev. C (to be published).
[15]M. A. Franey and W. G. Love, Phys. Rev. C **31**, 488 (1985).
[16]R. A. Arndt, program SAID (unpublished); R. A. Arndt, L. D. Roper, R. A. Bryan, R. B. Clark, B. J. VerWest, and P. Signell, Phys. Rev. D **28**, 97 (1983).
[17]M. W. McNaughton, Los Alamos Scientific Laboratory Report LA-8307, 1980.
[18]L. G. Atencio, J. A. Amann, R. L. Boudrie, and C. L. Morris, Nucl. Instrum. Methods **187**, 381 (1981).
[19]J. J. Kelly, computer program ALLFIT (unpublished).
[20]S. Dixit, W. Bertozzi, C. Hyde-Wright, J. Kelly, M. V. Hynes, B. E. Norum, J. M. Finn, M. A. Kovash, F. W. Hersman, A. D. Bacher, G. T. Emery, C. C. Foster, W. P. Jones, D. W. Miller, and B. L. Berman, Phys. Rev. C (to be published).
[21]F. Ajzenberg-Selove, Nucl. Phys. **A375**, 1 (1982).
[22]D. Lopiano, Ph.D. thesis, University of California at Los Angeles (in preparation).
[23]See AIP document no. PAPS PRVCA-43-1272-14 for 14 pages containing a complete tabulation of the data described in this paper. Order by PAPS number and journal reference from American Institute of Physics, Physics Auxiliary Publication Service, 335 E. 45th Street, New York, NY 10017. The price is $1.50 for each microfiche or $5.00 for photocopies. Air mail additional. Make checks payable to the American Institute of Physics.
[24]T. N. Buti, J. Kelly, W. Bertozzi, J. M. Finn, F. W. Hersman, C. Hyde-Wright, M. V. Hynes, M. A. Kovash, S. Kowalski, R. W. Lourie, B. Murdock, B. E. Norum, B. Pugh, C. P. Sargent, W.Turchinetz, and B. L. Berman, Phys. Rev. C **33**, 755 (1986).
[25]The ^{16}O density due to G. Lahm (Ph.D. thesis, University of Mainz, 1986) may be found tabulated in H. deVries, C. W. deJager, and C. deVries, At. Data Nucl. Data Tables **36**, 495 (1987).
[26]H. Miska, B. Norum, M. V. Hynes, W. Bertozzi, S. Kowalski, F.N. Rad, C. P. Sargent, T. Sasanuma, and B. L. Berman, Phys. Lett. **83B**, 165 (1979).
[27]T. Cheon, K. Takayanagi, and K. Yazaki, Nucl. Phys. **A437**, 301 (1985); **A445**, 227 (1985); T. Cheon and K. Takayangi, *ibid.* **A455**, 653 (1986).
[28]J. Hüfner and C. Mahaux, Ann. Phys. (N.Y.) **73**, 535 (1972).
[29]M. Lacombe, B. Loiseau, J. M. Richard, R. Vinh Mau, J. Cote, P. Pires, and R. de Tourreil, Phys. Rev. C **21**, 861 (1980).
[30]P. J. Siemens, Nucl. Phys. **A141**, 225 (1970).
[31]R. Machleidt, K. Holinde, and Ch. Elster, Phys. Rep. **149**, 1 (1987).
[32]K. M. Watson, Phys. Rev. **89**, 575 (1953).
[33]E. L. Lomon and H. Feshbach, Ann. Phys. (N.Y.) **48**, 94 (1968); E. L. Lomon, Phys. Rev. D **26**, 576 (1982).
[34]J. J. Kelly, Q. Chen, P. P. Singh, M. C. Radhakrishna, W. P. Jones, and H. Nann, Phys. Rev. C **41**, 2525 (1990).
[35]H. V. von Geramb, private communication.
[36]F. Petrovich, J. A. Carr, R. J. Philpott, A. W. Carpenter, and J. Kelly, Phys. Lett. **165B**, 19 (1985).
[37]H. Seifert, Ph.D. thesis, University of Maryland, 1990.
[38]M. V. Hynes, A. Picklesimer, P. C. Tandy, and R. M. Thaler, Phys. Rev. Lett. **52**, 978 (1984).
[39]C. J. Horowitz and B. D. Serot, Nucl. Phys. **A368**, 503 (1981).
[40]D. P. Murdock and C. J. Horowitz, Phys. Rev. C **35**, 1442 (1987).
[41]H. F. Arellano, F. A. Brieva, and W. G. Love, Phys. Rev. Lett. **63**, 605 (1989); Phys. Rev. C **41**, 2188 (1990).
[42]Ch. Elster and P. C. Tandy, Phys. Rev. C **40**, 881 (1989); Ch. Elster, T. Cheon, E. F. Redish, and P. C. Tandy, *ibid.* **41**, 814 (1990).
[43]N. Ottenstein, E. E. van Faassen, J. A. Tjon, and S. J. Wallace, Phys. Rev. C **42**, 1825 (1990).
[44]G. E. Brown, C. B. Dover, P. B. Siegel, and W. Weise, Phys. Rev. Lett. **60**, 2723 (1988); G. E. Brown and M. Rho, Phys. Lett. B **222**, 324 (1989); G. E. Brown, H. Müther, and M. Prakash, Nucl. Phys. **A506**, 565 (1990).